Hindawi
Shock and Vibration
Volume 2020, Article ID 7146828, 21 pages
https://doi.org/10.1155/2020/7146828

Research Article

Research on a Multinode Joint Vibration Control Strategy for Controlling the Steering Wheel of a Commercial Vehicle

Tao Tang,[1] **Shuilong He**,[1,2] **Mingsong Ye**,[2] **Enyong Xu**,[2] **and Weiguang Zheng**[1]

[1]*School of Mechanical and Electrical Engineering, Guilin University of Electronic Technology, Guilin 541004, China*
[2]*Dongfeng Liuzhou Motor Co., Ltd., Liuzhou 545005, China*

Correspondence should be addressed to Shuilong He; xiaofeilonghe@163.com

Received 27 August 2019; Revised 23 October 2019; Accepted 5 November 2019; Published 4 January 2020

Academic Editor: Stefano Manzoni

The vibration degree of a steering wheel has important reference significance for drivers to evaluate the ride comfort of the whole vehicle. To solve the jitter problem of the steering wheel of a commercial vehicle at idle speed, this work proposes a multinode joint vibration control strategy (MDVC) based on the associated vibration path of the steering wheel. Based on the analysis of the associated vibration transfer paths of the steering wheel, the whole vehicle was divided into a system comprising several nodes. For the decomposed node system, taking the vibration transmission path associated with the target as the research direction, the vibration reduction design of each node system is analyzed step by step. After exploring the possible causes of abnormal vibration of the steering wheel through experimental tests, the abnormal node structure interval was determined. By further extracting the structural model of the steering system from the vehicle, the hammering method was applied to test its modal and related frequency. Furthermore, an improved structure of steering support was also designed, and its fitting degree and modal characteristics were analyzed and compared to the original scheme. The following test results show that the structure improvement greatly reduces the vibration level of the steering wheel, meets the ideal design requirements of the steering wheel vibration reduction, and provides the possibility of weighing the correlation between these hierarchical node systems in whole vehicle.

1. Introduction

Recently, with the development of the transportation and logistics industry, the abnormal vibration problem of the steering wheel has attracted the attention of many drivers. Excessive direction jitter affects the driver's driving comfort and affects the driver's arm and spine, resulting in dizziness. Therefore, effectively reducing the vibration of the steering wheel is important for improving the driver's ride comfort.

Because structural components of the steering wheel are mainly sheet metal parts with a certain thickness, the overall structural damping of the steering system is small. Consequently, it can be ignored in the analysis and used as a scattered composite rigid body for resonance suppression analysis [1]. In the last two decades, researchers have performed many studies on the approaches for the resonance suppression of structure, not only simple design models [2–9] to adjust vibration control parameters, but also dynamic vibrational behaviour of the structure [10, 11]. In addition, other methods have been studied to regulate vibration responses. Among them, the finite element method (FEA) and modal analysis method are two ways to detect the vibration characteristics (i.e., vibration modes and modal frequencies) of structures. Because of their superior properties (i.e., accuracy, visibility, and convenience), they are widely used in the field of vibration characteristic detection of structures. EI-Gazzar [12] used the FEA to detect the variation of the vibration characteristics of the motor structure and the influence of the structural stiffness on the structural resonance. Tullu et al. [13] used the FEA to establish the propeller model and used the nonlinear sequence

quadratic programming algorithm to obtain the optimal parameters of the first fundamental frequency of the structure to avoid the resonance problem. Tompkins et al. [14] used the FEA to calculate the natural frequency of the pump structure and modeled the possible modifications to eliminate the harmful resonance effects. However, the FEA method is extremely dependent on the accuracy of the established model [15], and the simplification of some of the details of the model affects the accuracy of the model in vibration analysis [16]. Therefore, it is necessary to compare the accuracy and fitting degree of the finite element model by using the experimental modal analysis method [17, 18] to repair errors in the model. The joint application of these two methods makes the obtained structural model more accurate, thus obtaining more complete vibration modal information.

However, many defects existed in the methods listed above can be concluded as follows: one the one hand, the accurate mathematical model requires a large number of specific parameters in the model and the error between the parameter value and the actual model is also hard to meet the design standard. Because of the high complexity of mathematical modeling [19, 20] and too many external influencing factors [21]), dynamic digital modeling method is declined to rely on the design experience of designers, and the establishment of a complex isometric model for a complex multimember system requires a large design and adjustment period. The establishment and design of the dynamic parametric model brings good visualization and maneuverability to the complex model, and the modeling is less difficult and more coordinated and is better close to the real experimental environment. In some performance indicators, the dynamic parameter model is not only convenient for the unified design of the whole vehicle but convenient for the layered design of the whole vehicle, along with the simulation analysis and verification of the whole vehicle. On the other hand, for complex dynamic models, although some scholars use hierarchical decomposition method to complex model, there are few studies on the classification and systematic analysis of the vibration connection characteristics between the nodes of the hierarchical system of the complex vehicle model.

Therefore, in order to find a low-cost and easy modeling vibration control method [22, 23], along with an interactive analysis of vibration correlation between decomposed node systems. In this paper, a multinode joint vibration control strategy (MDVC) is proposed based on the node analysis of the vibration path of the steering system. By taking the steering wheel as the global objective of optimization analysis, the whole vehicle is graded into different node systems in turn on the basis of the established multibody model. Secondly, for different node systems, based on the consideration of resonance effect and vibration isolation effect, the contact relationship between nodes and the dependence between adjacent nodes are identified and classified. Then, on the basis of the vibration transfer path associated with the target object, a series of damping analyses are compared and analyzed according to the classification relationship of the node system. Through the comparative verification and analysis of the experiment, it is inferred that the abnormal vibration of the steering wheel is due to the modal frequency of the structure of the steering wheel is close to idling ignition excitation frequency of the engine. Furthermore, after the main vibration transfer path was determined based on the characteristic analysis of vibration transfer path related to the steering system, an independent steering model was extracted and studied. Referring to the steering model installed on the whole vehicle, the extracted steering model maintains the original constraints and inherent parameter attributes. The each joint of the steering system structure was identified as the node of each separated member in the analysis. In subsequent real vehicle tests, the vibration sensor was uniformly distributed on these nodes, and combined with the test data, the abnormal vibration link interval of the steering wheel and the corresponding engine excitation speed were found in turn under the condition of the idling test. Based on the studies on the redesign of the vibration parameters [24–26] and modal frequency offset optimization [27–29], the structures existing in these abnormal vibration link intervals further improved. After obtaining the vibration modal information with the FEA and modal analysis methods, along with the results of the actual vehicle test, the analysis results show that the overall modal frequency of the improved steering system deviated from the excitation frequency of the engine, realising the offset frequency damping design of the steering system and verifying the effectiveness of the improved scheme and MDVC.

The rest of this paper is organised as follows: in Section 2, the design principle and implementation process of MDVC is briefly introduced. Then, Section 3 analyzes the implementation process of MDVC. In addition, the vibration testing and stress analysis of an extracted steering wheel were performed, and a vibration reduction design of steering the fixed support for the steering system of nodes are introduced in Section 4. Furthermore, its effectiveness was verified by experiments in Section 5. Lastly, the conclusions are given in Section 6.

2. Principle of MDVC Methods

2.1. Analysis of the Correlated Vibration Transfer Path of the Steering Wheel. Because the vibration source of the idle vehicle is relatively single, producing benefits for clearly identifying the flow of the path, according to the dependence of the steering structure on the body, the complete steering vibration transmission path can be further detected, as shown in Figure 1.

Considering that the influencing factors of steering wheel vibration mainly come from the inertia resonance excitation transfer effect and ignition pulse excitation of the engine, the vibration path of steering wheel vibration shown in Figure 1 can be summarised as follows:

(a) Engine-engine mount–frame–cab–steering fixed support–steering wheel

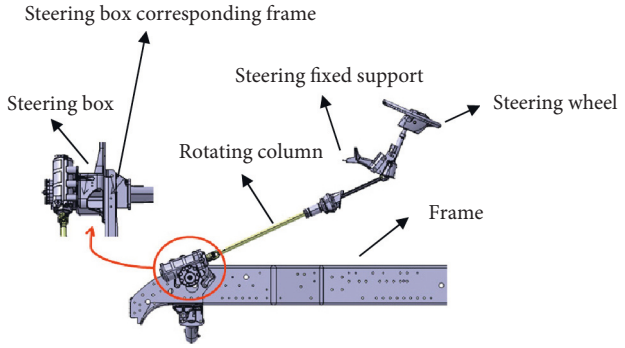

Figure 1: Steering wheel associated vibration path.

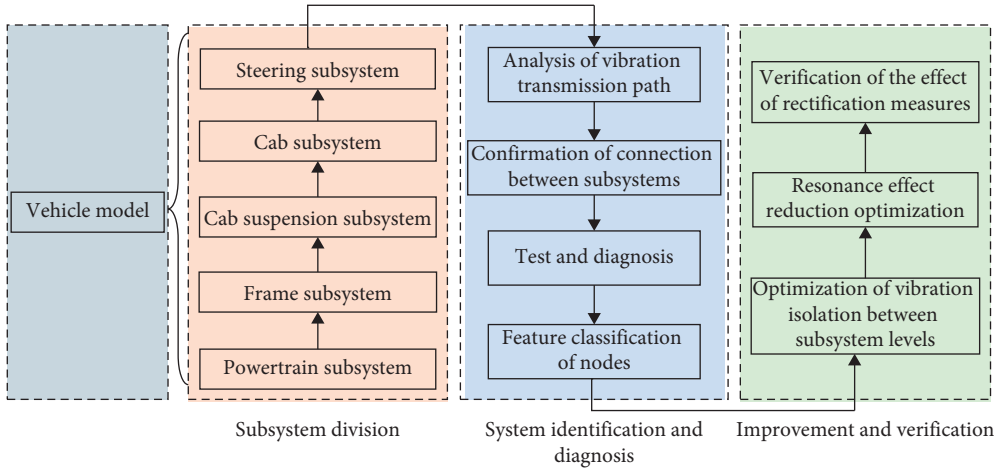

Figure 2: Method implementation flow chart.

(b) Engine-engine mount–frame–steering box–steering box corresponding frame–rotating column–steering fixed support–steering wheel

Therefore, based on the complete vibration transfer path analysis of the "vibration source-vibration transfer path-response source," the improvement means of the vibration node system mainly include the engine mount, the steering fixed support, rotating column, steering wheel, and frame.

2.2. Analysis of Vibration Transmission Characteristics. According to the existing steering transmission path, because of the large number of components connected by the complete steering structure, it is inevitable to avoid interference and coupling of vibration signals on different vibration transmission paths. Therefore, the total vibration transfer energy of the whole branch path can be evaluated by the vibration level of the connecting nodes (coupling points) of each branch of the vibration transfer path, helping avoid the interference of other coupling signals received in the small branches of vibration transmission paths, and the vibration signal of the joint coupling point between different components can be used as the node to separate each component system, as shown in Figure 2.

As shown in Figure 2, the subsystems of the steering wheel vibration history are divided according to the vibration transmission path direction of "excitation source-vibration transfer path target object." After confirming the distribution position relationship and characteristics of the node system, the characteristics of each node system can be further analyzed to make an improved design analysis of adaptability.

For a complete vibration transmission path, more vibration branches make vibration detection much more complicated. When the contribution ratio of vibration energy on one vibration path is much higher than that of other vibration branch paths, the vibration energy on this vibration path is disturbed by the noise of other vibration paths (such as the interference loss of vibration energy and the generation of resonance self-excited energy) and can be used as the main vibration transfer chain to express the original vibration system model formed by multi-vibration branches. As shown in Figure 3, we divide the vibration transfer path into several subsystems (i.e., node systems 1, 2, 3, and 4) according to the structure of the actual steering system. In terms of system types, each node system is divided as different transfer structure system types.

2.2.1. Node System 1. This node system is connected with other node systems through several vertical fulcrums (i.e.,

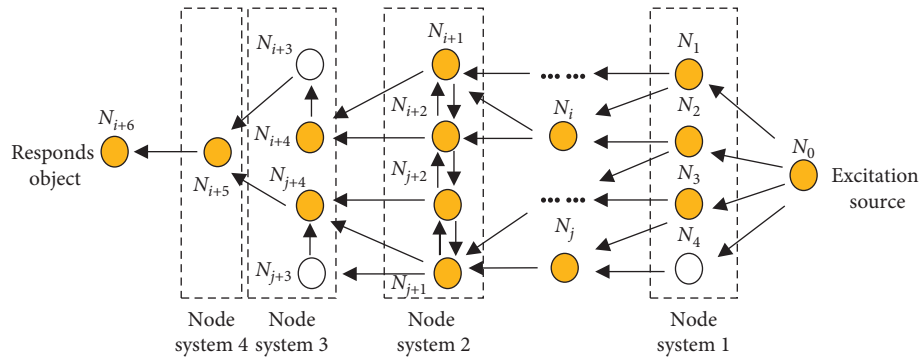

Figure 3: Division of the node system of the vibration transfer chain.

the joint point on the mounting fulcrum of the engine). When the vibration is transmitted from other vibration node systems, the vibration is transferred directly to the structure body through these fulcrums. The vibration deformation generated by the structure body consumes the vibration internally, and there is no coupling of vibration between the internal subpath structures. The following equation shows the relationship between the vibration velocity response V_A of the structural ontology, the admittance transfer function H_A, and the exciting force F_A:

$$\{V_A\} = [H_A]\{F_A\}. \tag{1}$$

Because the vibration of each connected coupling node on the structural body is relatively independent (assuming that the equilibrium parameter characteristics caused by the rubber bushing itself are ignored), the decomposition component $(H_i, F_i, V_i, i = 1, 2, 3)$ of (V_A, H_A, F_A) on each coupling node (N_1, N_2, N_3) can be expressed as follows:

$$[H_A] = \begin{bmatrix} H_1 & & \\ & H_2 & \\ & & H_3 \end{bmatrix},$$

$$F_A = \begin{bmatrix} F_1 & & \\ & F_2 & \\ & & F_3 \end{bmatrix}, \tag{2}$$

$$V_A = \begin{bmatrix} V_1 & & \\ & V_2 & \\ & & V_3 \end{bmatrix}.$$

2.2.2. Node System 2. The node system contains many discrete structures with low constraint, and a series of vibrator transfer paths are formed by relying on the dynamic oscillation behaviour of the discrete structure (i.e., the vibration transmission of four-point suspension to the cab rigid body). The balance ability of the mounting parameters in the vibration behaviour determines the main vibration mode direction and vibration intensity. In this kind of node system, while considering the vibration coupling relationship between each discrete structure and the structure body, the corresponding vibration transfer variables of the whole vehicle can be expressed as follows:

$$\{V'_A\} = [H'_A]\{F'_A\},$$

$$[H'_A] = \begin{bmatrix} [H_1]_{R,R} & [H_1]_{R,S1} & \cdots & [H_1]_{R,Sn} \\ [H_1]_{S1,R} & \cdots & & \cdots \\ \cdots & & \cdots & \cdots \\ [H_1]_{Sn,R} & \cdots & \cdots & [H_1]_{Sn,Sn} \end{bmatrix},$$

$$F'_A = \begin{bmatrix} F_R & & & \\ & F_{S1} & & \\ & & \cdots & \\ & & & F_{Sn} \end{bmatrix}, \tag{3}$$

$$V'_A = \begin{bmatrix} V_{R1} & & & \\ & V_{S1} & & \\ & & \cdots & \\ & & & V_{Sn} \end{bmatrix}.$$

2.2.3. Node System 3. The node system contains a small number of structural combinations (such as rigid connections between the steering gear and frame) that are rigidly connected between rigid bodies. At the rigid connection point, because of the influence of vibration transmission from different components, the vibration signal types of the connection point are more concentrated and the signal strength is more obvious. Therefore, the vibration signal at the rigid connection point can be used as the main node of the subsystem and the location of the measuring point for analyzing the vibration test. In analyzing the coupling node system, these coupling nodes can be combined with other relatively independent nodes, and the related vibration transfer characteristics can be expressed as follows:

$$\left\{V_A^{''}\right\} = \left[H_A^{''}\right]\left\{F_A^{''}\right\},$$

$$\left[H_A^{''}\right] = \begin{bmatrix} [H_1]_{R,R} & [H_1]_{R,T_1} & \cdots & \cdots & [H_1]_{R,T_{i+1}} & & & \\ [H_1]_{T_1,R} & [H_1]_{T_1,T_1} & & & \cdots & & & \\ \cdots & & \cdots & & \cdots & & & \\ \cdots & & & [H_1]_{T_i,T_i} & [H_1]_{T_i,T_{i+1}} & & & \\ [H_1]_{T_{i+1},R} & \cdots & \cdots & [H_1]_{T_{i+1},T_i} & [H_1]_{T_{i+1},T_{i+1}} & & & \\ & & & & & [H_1]_{D_1,D_1} & & \\ & & & & & & \cdots & \\ & & & & & & & [H_1]_{D_n,D_n} \end{bmatrix},$$

$$F_A^{''} = \begin{bmatrix} F_R & & & & & & & \\ & F_{T_1} & & & & & & \\ & & \cdots & & & & & \\ & & & F_{T_i} & & & & \\ & & & & F_{D_1} & & & \\ & & & & & \cdots & & \\ & & & & & & \cdots & \\ & & & & & & & F_{D_n} \end{bmatrix}, \tag{4}$$

$$V_A^{''} = \begin{bmatrix} V_R & & & & & & & \\ & V_{T_1} & & & & & & \\ & & \cdots & & & & & \\ & & & V_{T_i} & & & & \\ & & & & V_{D_1} & & & \\ & & & & & \cdots & & \\ & & & & & & \cdots & \\ & & & & & & & V_{D_n} \end{bmatrix}.$$

2.2.4. Node System 4. The vibration transmission of this node system (i.e., part of the nodes distributed on the frame) mainly exists on the surface of the rigid body; thus, the vibration path is single. Because the mutual vibration coupling influence of the adjacent nodes (i.e., $X_1, X_2, \ldots, X_i$) is under single vibration excitation, the vibration transfer characteristics of this system of nodes can be shown as follows:

$$\begin{aligned}
\left\{V_A'''\right\} &= \left[H_A'''\right]\left\{F_A'''\right\},\\
\left[H_A'''\right] &= \begin{bmatrix}
[H_1]_{R,R} & [H_1]_{R,X_1} & & & & & & & & \\
[H_1]_{X_1,R} & [H_1]_{X_1,X_1} & & & & & & & & \\
 & & [H_1]_{X_2,X_2} & [H_1]_{X_1,X_2,X_3} & & & & & & \\
 & & [H_1]_{X_3,X_2,X_1} & [H_1]_{X_3,X_3} & & & & & & \\
 & & & & [H_1]_{X_4,X_4,X_4} & [H_1]_{X_1,X_2,X_3,X_4} & & & & \\
 & & & & [H_1]_{X_4,X_3,X_2,X_1} & [H_1]_{X_5,X_5,X_5} & & & & \\
 & & & & & & \cdots & & & \\
 & & & & & & & & [H_1]_{X_i,X_i,X_i}
\end{bmatrix},\\
V_A''' &= \begin{bmatrix}
V_R & & & & & & \\
 & V_{X_1} & & & & & \\
 & & \cdots & & & & \\
 & & & \cdots & & & \\
 & & & & \cdots & & \\
 & & & & & \cdots & \\
 & & & & & & V_{X_i}
\end{bmatrix},\\
F_A''' &= \begin{bmatrix}
F_R & & & & & & \\
 & F_{X_1} & & & & & \\
 & & \cdots & & & & \\
 & & & \cdots & & & \\
 & & & & \cdots & & \\
 & & & & & \cdots & \\
 & & & & & & F_{X_i}
\end{bmatrix}.
\end{aligned} \tag{5}$$

According to the existing equal node system classification method, the vibration transmission path of the vehicle steering system is divided based on the corresponding nodes, as shown in Figure 4.

According to the complete vibration transmission path and direction, the steering correlation system is divided into many different subsystems by the corresponding coupling nodes, mainly including the steering subsystem, cab mounting subsystem, and powertrain subsystem, and further analyses relying on these subsystems were performed.

3. Application of the MDVC Method

From the analysis of the main vibration paths associated with the steering wheel, the structure on the transfer path is divided and the node types are identified in turn. According to the node type of the decomposition subsystem, different rectification schemes can be adopted to avoid the influence of single node system rectification on other subsystems on the transfer path. Therefore, in order to improve the vibration isolation ability on the vibration transmission path, by taking the vibration of the steering wheel as the vibration target, the different node systems passing through the path are analyzed and optimized according to the direction of vibration transmission, and the optimization and modification of each system is analyzed, as shown below.

3.1. Modal and Decoupling Analysis of Powertrain Node Subsystem (Node System: Type 2). On the premise of shutting down the fan and other rotating excitation sources, the engine is the main excitation source under the idle condition. In terms of connection, the engine is mainly connected with the frame by mounting nodes n_1, n_2, and n_3 (shown in Figure 5). When the engine itself is unbalanced, it will seriously affect the vibration transmission value of each point on the transmission path and then affect the vibration degree of the steering wheel, so the balance control of the engine itself needs to be considered. Among them, the decoupling rate of the engine in six directions is an important index of

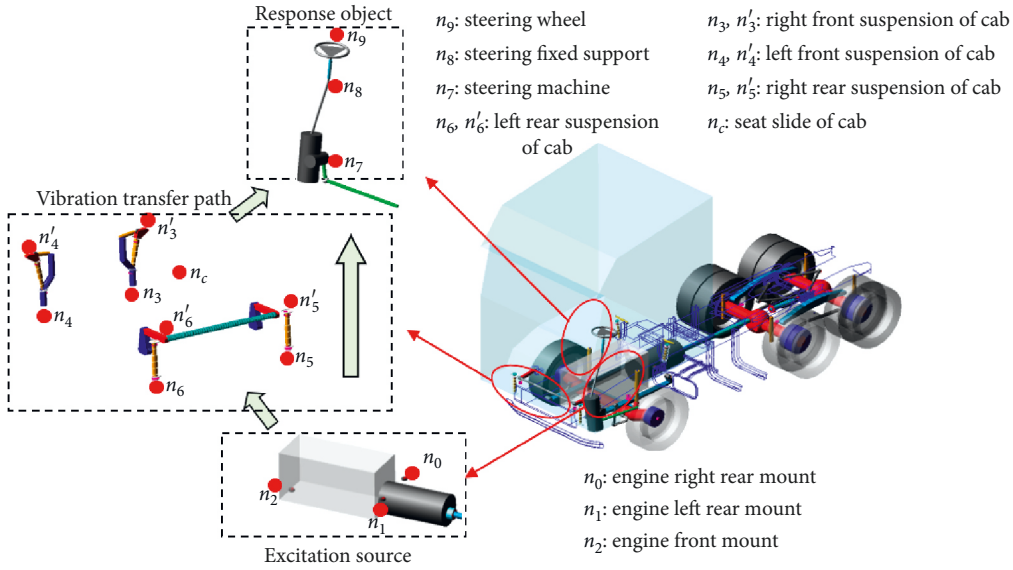

Figure 4: Node system division based on the vibration transfer path of the steering system.

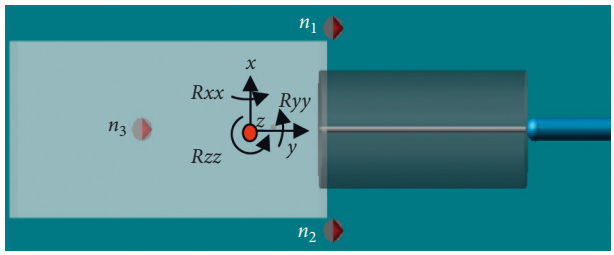

Figure 5: Six-direction decoupling and mounting node position of the engine.

the ontology balance of the reference engine. When the decoupling rate of all sides is insufficient, it is easy to affect the decoupling ability of the engine mounting system and greatly reduces the vibration isolation ability of the engine.

Through the modal analysis of the powertrain system, the distribution ratio of the vibration energy and the decoupling rate of the engine in the powertrain system are obtained, as shown in Figure 6.

As shown in Figure 6, in the overall vibration mode distribution ratio of the powertrain, the proportion of the engine exceeds 70% in all directions, so it is the main research object affecting the powertrain mode. In addition, with reference to the results shown in Table 1, compared with the engine body, its own decoupling rate in each direction is more than 95%, indicating that the vibration decoupling ability in each direction is better. Thus, it is very likely to explain the superiority of the vibration isolation ability of the engine and indicated that the engine is not the main reason that affects the abnormal vibration of the steering wheel.

3.2. Optimal Design of Cab Mounting Subsystem (Node System: Type 2). Cab mounting as a buffer of the cab, its upper and lower four fulcrums are connected to the frame and the cab, respectively. However, because there is no direct contact between the front and rear damping parts and the rear spring parts, the stability of this discrete arrangement can easily affect the damping capacity of the front and rear damping parts in the operating conditions. Therefore, the vibration reduction design of the original mounting structure is needed to be further analyzed. On the premise of the abnormal vibration problem of the steering wheel, the damping characteristic curves of the front and rear dampers and the spring are further matched. And the root-mean-square (RMS) value of the vibration acceleration (marked as a_i) of the steering wheel in the three-axis direction (x, y, z) is taken as the design goal, and the specific expression of which is shown as follows [30–33]:

$$a_i = \left[\frac{1}{T}\int_0^T a_w^2(t)\mathrm{d}t\right]^{1/2}, \tag{6}$$

$$a_w = \left[\int_{k_2}^{k_1} w_k^2(f)T(f)\mathrm{d}f\right]^{1/2}, \tag{7}$$

where a_w is the vibration acceleration time-domain signal and T is the recorded acceleration time. $T(f)$ is the unweighted acceleration power, $w(k)$ is the vertical vibration frequency weighting function, f is the vibration frequency, and (k_1, k_2) is the upper and lower limits of frequency. The rematching analysis of the front and rear damping characteristics and the damping characteristics of the spring is carried out in turn. Taking the RMS value of the steering wheel in the x direction as an example, the iterative optimization process is shown in Figure 7.

After 38 iterations of analysis, the optimal characteristic values of the damper and the spring are obtained under the minimum vibration value of the steering wheel. Among them, the response surface of some of the characteristic parameters to the acceleration of the steering wheel is shown in Figure 8.

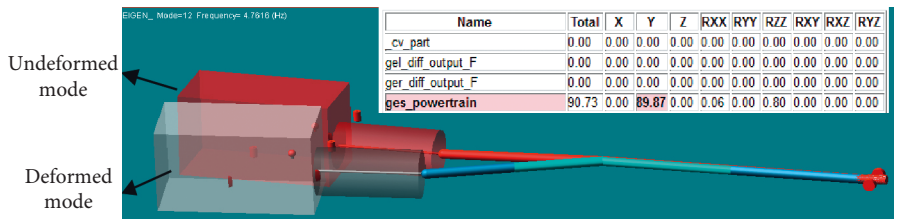

(a)

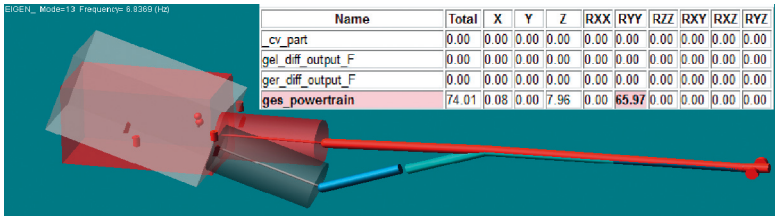

(b)

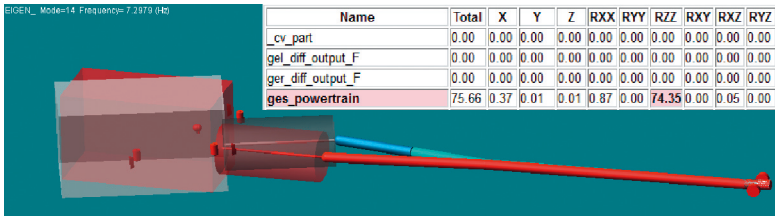

(c)

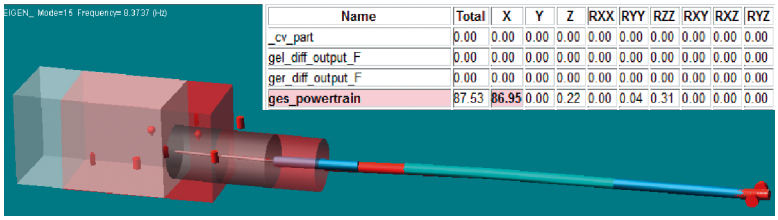

(d)

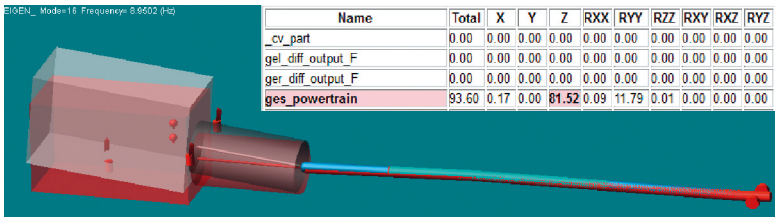

(e)

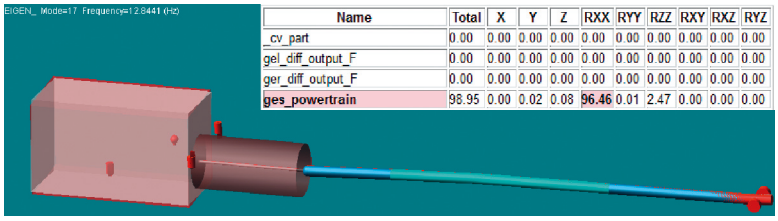

(f)

Figure 6: Modal kinetic energy distribution ratio and decoupling rate in all directions of the engine in powertrain system, which includes the decoupling rate on (a) *Y* direction, (b) *Ryy* direction, (c) *Rzz* direction, (d) *X* direction, (e) *Z* direction, and (f) *Rxx* direction.

By extracting the attribute value corresponding to the local optimal point on each response surface, the optimal matching characteristic curve is obtained and shown in Figure 9.

Furthermore, after replacing the damping matching characteristic curve shown in Figure 9 on the whole vehicle model, in order to verify the influence of the matching characteristic curve with the steering wheel as

Table 1: Decoupling rate distribution in all directions.

Direction	Modal energy distribution ratio (%)	Decoupling rate relative to powertrain system (%)	Decoupling rate relative to engine (%)
X	87.53	86.95	99.34
Y	90.73	89.87	99.05
Z	93.6	81.52	0.87
Rxx	98.95	96.46	97.5
Ryy	74.01	65.97	89.14
Rzz	75.66	74.35	98.27

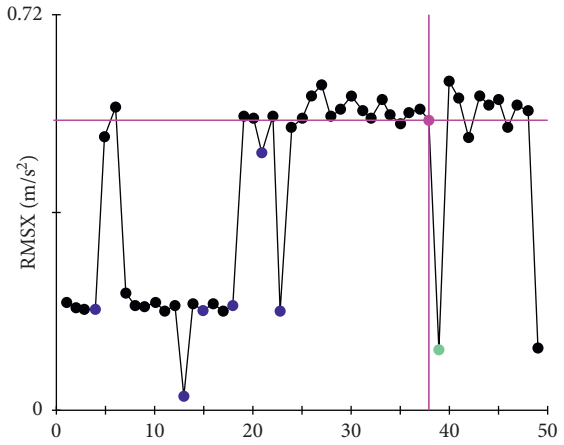

Figure 7: Iterative calendar of the RMS value optimization in the *x* direction of the steering wheel.

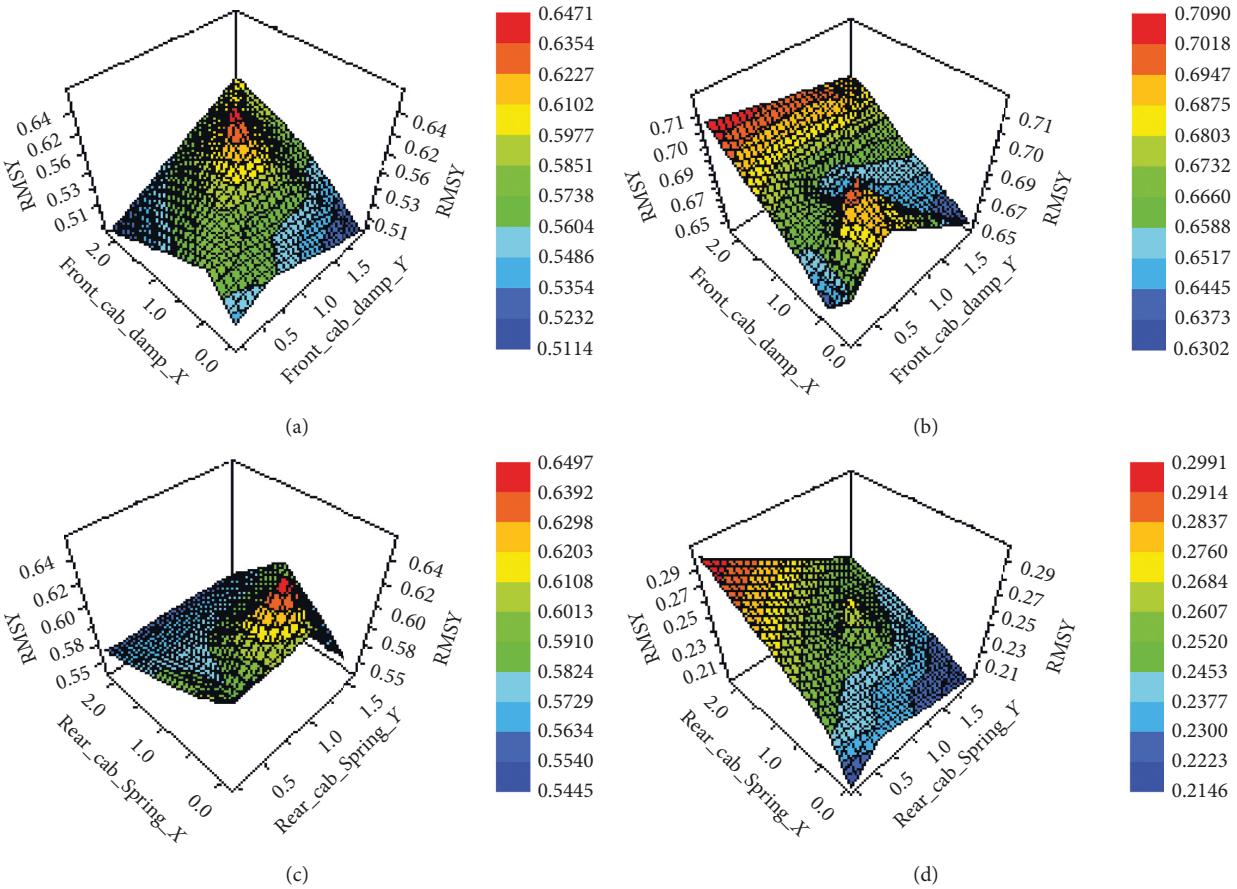

Figure 8: Response surface model of partial cab mounting parameters to steering wheel vibration, which included (a) effect of front suspension damping of cab on *y* direction vibration, (b) effect of front suspension damping of cab on *x* direction vibration, (c) effect of rear suspension spring damping of cab on *x* direction vibration, and (d) effect of rear spring damping of cab on *z* direction vibration.

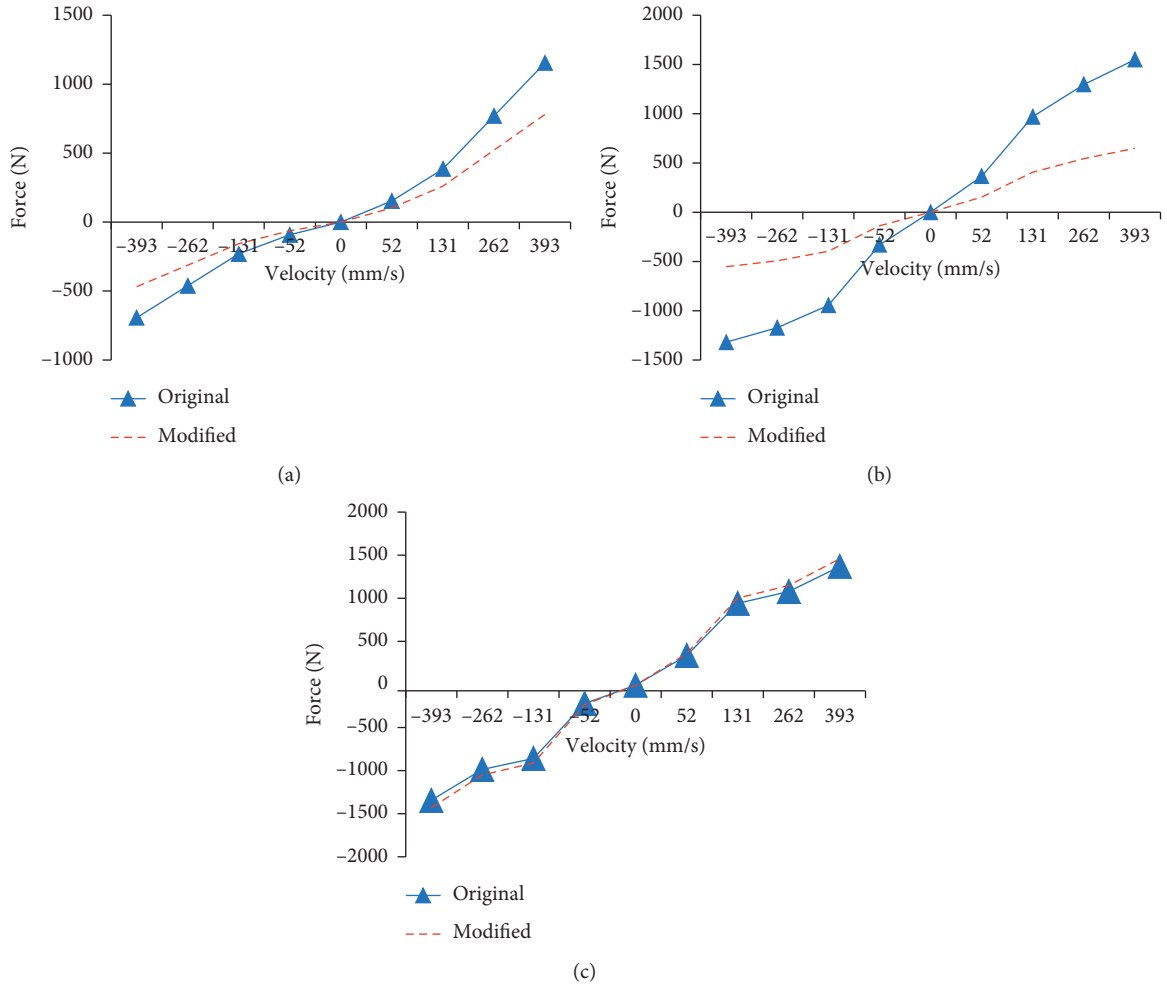

Figure 9: Comparison of nonlinear damping characteristic curves of (a) cab front suspension, (b) cab rear suspension, and (c) cab rear suspension.

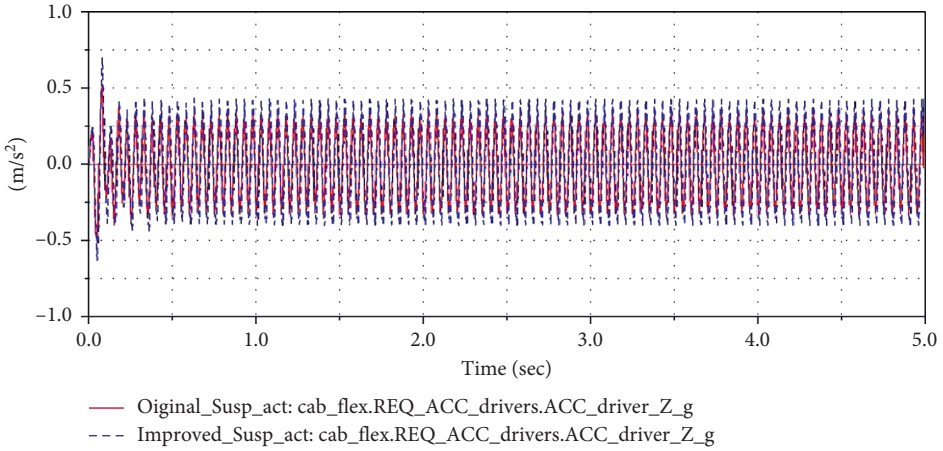

Figure 10: Acceleration time-domain spectrum of the cab seat.

the optimization target on the overall vibration of the cab. We further measured the measuring points at the cab seat during the test, and the results are shown in Figure 10.

As can be seen from Figure 10, the vibration intensity of the improved cab seat is greatly reduced compared with the original level, indicating that the optimization of the matching cab mounting characteristics is globally positive

on the whole vehicle and avoids inverse interference to other systems. Thus, the vibration control of the steering wheel is focused on the control of the components of the steering wheel node system.

4. Experimental Test and Analysis

To further substantiate the effects of the vibration transfer path associated with the steering wheel, a multinode distributed vibration control design strategy was introduced to realise the vibration control of the steering wheel.

4.1. Idle Vibration Test and Result Analysis. By considering the actual structural connection of the vibration transmission path of the steering system, the direct vibration transmission of the steering system results from the cab subsystem and the influence of the frame because of its direct vibration transmission. To identify which subsystem of nodes affects the steering wheel abnormal vibration, the corresponding idle vibration experiment was performed. In the windless and dry environment, the test acquisition equipment included a 24-bit CPCI (compact peripheral component interconnect) data acquisition instrument, electric measuring computer, and triaxial accelerometers. In addition, some of the measuring points of the steering wheel vibration test are shown in Figure 11.

As shown in Figure 11, in the preparatory phase of the experiment, the accelerometer was evenly placed at each measuring point of the steering wheel associated with the vibration path. During the test, the driver waited for each sampling speed to stabilise before collecting the signal and recording the working condition of each speed and the corresponding test number. The initial idle speed in the experiment was set to 650 rpm, and the stable speed interval was gradually increased by 50 rpm (maintained a sampling time for 20 seconds) until the final speed of the whole vehicle reached 1050 rpm. Then, the experiment was stopped, and the collected acceleration signal was further preprocessed and analyzed (including denoising and Fourier transform processes). According to formula (6) and because the initial speed of the engine is usually between 600 and 800 rpm, the corresponding vibration data collected by each measuring point can be converted to RMS, and the results are shown in Figures 12–14.

The results in Figure 12 show that, on the one hand, the sharp vibration RMS value increases when the idle speed changes from 700 to 750 rpm, while on the other hand, when the idle speed is 800 rpm, the RMS value decreases rapidly, so the resonance effect is produced in the abnormal node structure interval from the steering fixed support to the steering wheel when the idle speed is between 700 and 750 rpm. In addition, the vibration transmission degree on the engine mounting nodes (n_1, n_2, n_3) can be determined by the vibration isolation rate δ_t, which is mainly calculated by the ratio between the vibration-excited RMS value generated by the engine body and the vibration RMS values of the front, the left rear, and the right rear mounts, as follows [34, 35]:

$$\delta_{t_1} = \frac{a_{n_1}}{a_p} \times 100\%,$$

$$\delta_{t_2} = \frac{a_{n_2}}{a_p} \times 100\%, \tag{8}$$

$$\delta_{t_3} = \frac{a_{n_3}}{a_p} \times 100\%,$$

where a_p is the vibration RMS value of the engine body and a_{n1}, a_{n2}, and a_{n3} are the vibration RMS values of the front mount of the engine, left rear mount of the engine, and right rear mount of the engine, respectively. Thus, the vibration transmission level of the mount can be estimated, and the results are shown in Figure 13. The results show that the vibration isolation rate of the mount is more than 70%, agreeing with the vibration isolation standard of the mount; consequently, the influence of vibration excitation of the engine body is eliminated. In addition, according to the vibration data shown in Figure 14, there is no vibration amplification between the upper and lower nodes of the suspension, and the vibration RMS at the cab seat also meets the requirements of the vibration standard value ($0.4\,\mathrm{m/s^2}$), which is calculated by the GB_T 18707.1-2002 standard.

In general, the resonance effect of the system of cab nodes and the damping defect of the cab suspension structure, along with the effect of vibration transfer excitation on the engine, are excluded. Furthermore, because the steering node system is mostly a rigid body combination structure, the damping value is too small. Consequently, the damping effect of the steering node system is weak, and the possible influence of the self-excited resonance effect of the steering node system on the steering wheel vibration is further studied in the next section.

4.2. Analysis of Damping Design of Steering Node System

4.2.1. Ignition Excitation Analysis of Engine Node System. On the one hand, under idle operating conditions, the engine (four-stroke) is the main excitation source affecting the vibration of the steering wheel. The main excitation of the engine mainly comes from the torsional pulsation caused by changes in the internal cylinder pressure and can be expressed by the ignition pulse vibration excitation, and the corresponding calculation equation is as follows [36]:

$$f_{si} = \frac{ni}{60\tau}, \quad n \in (600\,\mathrm{rpm}, 650\,\mathrm{rpm}, \ldots, 1200\,\mathrm{rpm}), \tag{9}$$

where n is the rotation speed of the engine, i is the number of cylinders, and τ is the number of strokes of the engine. When the whole vehicle is driving at idle speed n, the engine excitation frequency range corresponding to each sample speed can be expressed as follows:

$$f_s = (f_{s1}, f_{s2}, f_{s3}, \ldots, f_{sn}), \tag{10}$$

where f_s is the ignition frequency of the engine and f_{s1}, f_{s2}, …, f_{sn} represent the ignition frequencies of engine corresponding to specific rotational speed (600 rpm, 650 rpm,

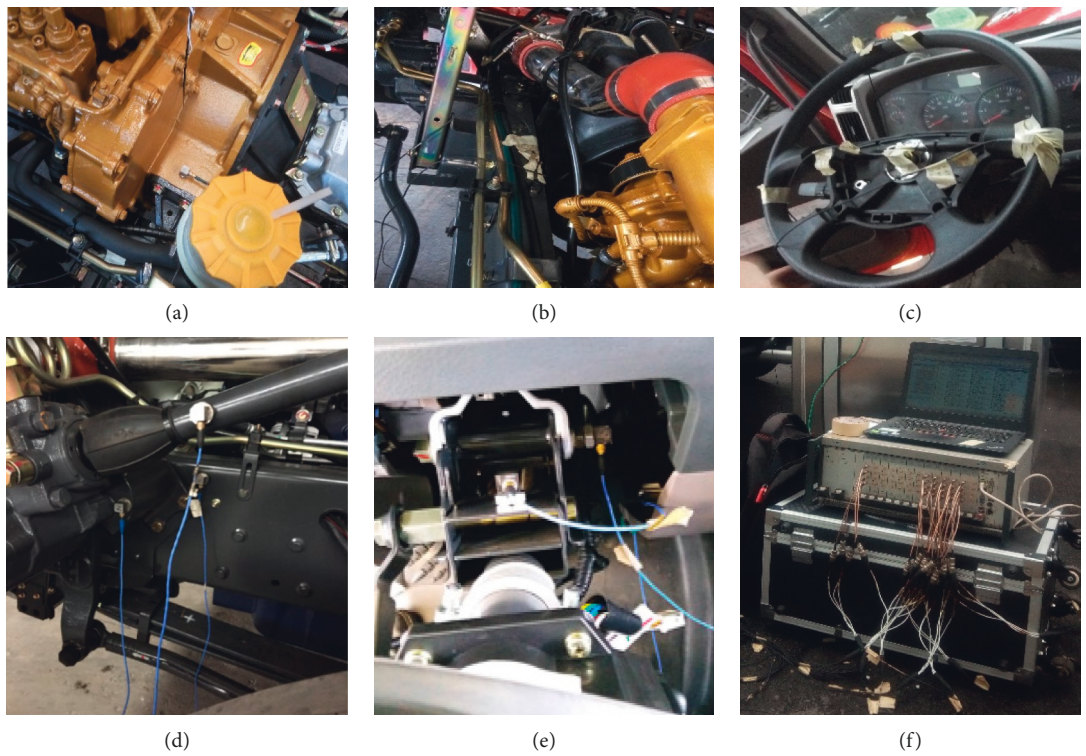

Figure 11: Arrangement of experimental measuring points: (a) engine, (b) frame, (c) steering wheel, (d) steering box and steering box corresponding frame, (e) steering fixed support, and (f) test acquisition equipment.

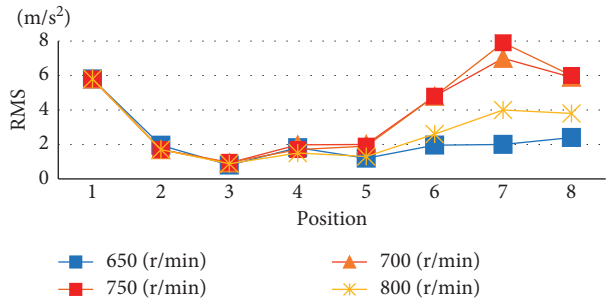

Figure 12: RMS of vibration extracted from each measuring point on the steering wheel-associated vibration path.

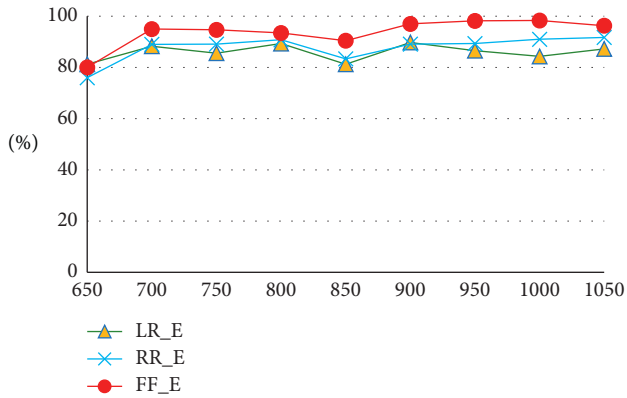

Figure 13: Vibration isolation rate of the engine three-point mount.

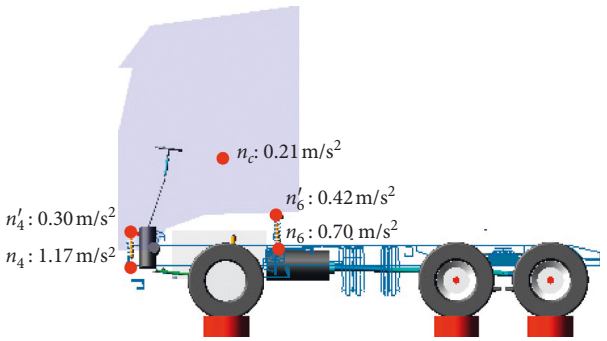

Figure 14: RMS value of the measuring point on the cab mounting subsystem.

700 rpm, . . ., 1200 rpm). Because the fuel produces mostly unevenly mixed combustion, the vibration excitation is also different. Among the vibration excitation forms, the excitation disturbance of ignition frequency is the main form, so it is necessary to study the vibration isolation ability of the excitation disturbance of ignition frequency. According to the determined abnormal idle speed, a corresponding ignition frequency range can be further calculated according to equation (9), and its range varies from 23.3 Hz to 25 Hz.

In contrast, for any other node system structure (suppose the number of components contained in this system of nodes is 4), the natural frequency (w_i) is mainly determined by the stiffness and mass and is not affected by external vibration. Considering the mass and stiffness distribution of the multi-degree-of-freedom joint structure system, the undamped system vibration can be approximately determined:

$$\begin{pmatrix} m_1 & & & \\ & m_2 & & \\ & & m_3 & \\ & & & m_i \end{pmatrix} \begin{Bmatrix} \Delta\ddot{x}_1 \\ \Delta\ddot{x}_2 \\ \Delta\ddot{x}_3 \\ \Delta\ddot{x}_i \end{Bmatrix} + \begin{pmatrix} k_1 & & & \\ & k_2 & & \\ & & k_3 & \\ & & & k_i \end{pmatrix} \begin{Bmatrix} \Delta x_1 \\ \Delta x_2 \\ \Delta x_3 \\ \Delta x_i \end{Bmatrix} = \begin{Bmatrix} 0 \\ 0 \\ 0 \\ 0 \end{Bmatrix}. \tag{11}$$

Assuming that the mass and stiffness of components in the system of nodes are balanced in dynamic vibration and the response is stable, the kinematic displacement solution of the equation can be established as follows:

$$X_i = A^{(t)} \sin\left(w_{ni} t + \varphi_i\right), \tag{12}$$

where

$$X_i = \begin{Bmatrix} \Delta x_1 \\ \Delta x_2 \\ \Delta x_3 \\ \Delta x_i \end{Bmatrix}, \qquad A^{(t)} = \begin{pmatrix} A_1^{(i)} \\ A_2^{(i)} \\ A_3^{(i)} \\ A_i^{(i)} \end{pmatrix}, \tag{13}$$

where $A_1^{(i)}$, $A_2^{(i)}$, $A_3^{(i)}$, and $A_4^{(i)}$ are represent the displacement amplitude of Δx_1, Δx_2, Δx_3, and Δx_4, respectively; w_{ni} is the natural frequency of i-th mode; and φ_i is the phase angle of the i-th mode, respectively. Furthermore, the vibration characteristic equation of the system can be obtained as follows:

$$\left|H^{(i)}\right| = \begin{vmatrix} k_1 - w_{n1}^2 m_1 & & & \\ & k_2 - w_{n2}^2 m_2 & & \\ & & k_3 - w_{n3}^2 m_3 & \\ & & & k_i - w_{ni}^2 m_i \end{vmatrix} = 0. \tag{14}$$

By solving the above polynomial, the distribution frequency of the multiorder structure can be further obtained, yielding the following relationship:

$$0 \le w_{1n} \le w_{2n} \le \ldots \le w_{in}, \tag{15}$$

where w_{in} represent the i-th order natural frequencies of the n-th rigid member. In addition, because the low-order mode accounts for a large proportion of the whole vibration modes, for example, the first five secondary modes account for 90% of the total vibration modes, the low-order modes contain more complete vibration information. Therefore, the frequency range of low order should be considered and can be expressed as

$$w_n \in \left(w_{i1}, w_{i_2}, \ldots, w_{in}\right), \quad i \le 5, n \le 4. \tag{16}$$

By considering the inertia torque caused by the rotation of the crankshaft inside the engine, the periodic inertia force is produced and radiates in the circumferential direction. At this time, each component in the node system produces a certain displacement offset (Δx_v, Δx_1, Δx_2, Δx_3, and Δx_R). In addition, the wide excitation frequency band generated by the engine interacts with the natural frequency bandwidth determined by the mass (m_1, m_2, m_3, and m_R) and stiffness (k_1, k_2, k_3, and k_R) of the system of nodes, inevitably producing additional vibration displacement (δ_1, δ_2, δ_3, and δ_R) under the mutual coupling of the excitation frequency of the engine. Therefore, the associated parameters corresponding to each node system can be represented as

$$\begin{aligned} S_{(1,2,3,\ldots,i)}\colon x = \Delta x_i \pm \delta_1, \quad \text{when } w_i \in \left(0.707 * w_s, 1.414 * w_s\right), \\ k_{\min} \le k_1 \le k_{\max}, \\ m_{\min} \le m_1 \le m_{\max}. \end{aligned} \tag{17}$$

Combining our results with the existing analysis and correlation parameter research, the vibration control design goal of the steering wheel can be set as two main categories: (a) the possible resonance effect can be avoided by realising the frequency offset of the rigid structure; (b) although the members of the steering wheel are mostly rigid body structures, considering the damping effect of the curved plate [37, 38], the damping characteristics of the structural parameters between these components can be set as c_i and used to optimize the damping capacity between these structural components and help improve the vibration isolation capacity of the vibration transfer path. In addition, the damping subdesign model of the steering system can be expressed as follows:

$$\begin{aligned} f_i(x)\colon \ & \min R + \max\left(w_s - w_i\right), \\ & k_{i-1} \le k_i \le k_{i+1}, \\ & m_{i-1} \le m_i \le m_{i+1}, \\ & c_{i-1} \le c_i \le c_{i+1}, \\ & w_i \ge 1.414 * w_s, \\ & \text{or } w_i \le 0.707 * w_s, \end{aligned} \tag{18}$$

where R represents the root-mean-square values of vibration weighted acceleration of the transfer node, w_s represents the excitation frequency of an engine at a certain idle speed, and w_i represents the proximity value of the natural frequency of a node system. For specific damping design objectives, c_i is an effective constrained damping value in the constraint range $[c_{i-1}, c_{i+1}]$. Similarly, k_i and m_i are the important design parameters for frequency offset design in the corresponding constrained range.

4.2.2. Extraction of Steering Node System Model. When the driving speed of the vehicle lies in an abnormal idle range, the main node structure interval of abnormal vibration is between the rotating column and the steering wheel. To obtain the complete vibration mode and modal information of the steering system model, a solid steering model is further extracted from the studied vehicle, and the hammering method is also applied to research the inherent characteristics of the solid steering model, as shown in Figure 15.

Based on the extracted steering system model, to obtain a more complete modal vibration (such as mode shape and frequency) of the steering model, many accelerometers were evenly arranged on the steering model in the position shown in Figure 16.

The measuring points were placed on the deformed nodes of the corresponding simulation model, and the distance between the measuring points should be in accordance with the structural characteristics of the steering wheel system, and there should be no interference and position interleaving to avoid the occurrence of errors. Furthermore, the multipoint hammering method [39, 40] is used to hammer the steering model with interval uniformity to detect the change of vibration modal properties of the model as a whole. In addition, the intensity of each hammer is consistent, and the position and direction of the hammer are shown in Figure 17.

Under the limitation of local coordinate systems x, y, and z, the force hammer excites the steering wheel and the rotating column structure with the same intensity, and the vibration response data of the steering wheel system are obtained. Because the proportion of the modal participation of the low-order mode is much higher than that of the high-order mode, the first several modes of the steering model are extracted for comparative verification and analysis.

In fact, the lower mode frequency of nodes systems is nearly equal to its own natural frequency, and the modal test results shown in Figure 18 shows that the first-order modal frequency of the steering model is close to the ignition pulse frequency of the engine, indicating it is easy to cause steering system resonance problems.

4.3. Vibration Reduction Design of Steering Fixed Support. According to the inherent properties of a rigid body structure, because the steering system is mostly a rigid body structure, it can be equivalent to an undamped rigid body system. In the isolation analysis of the structures

Figure 15: Extracted solid model of the steering system.

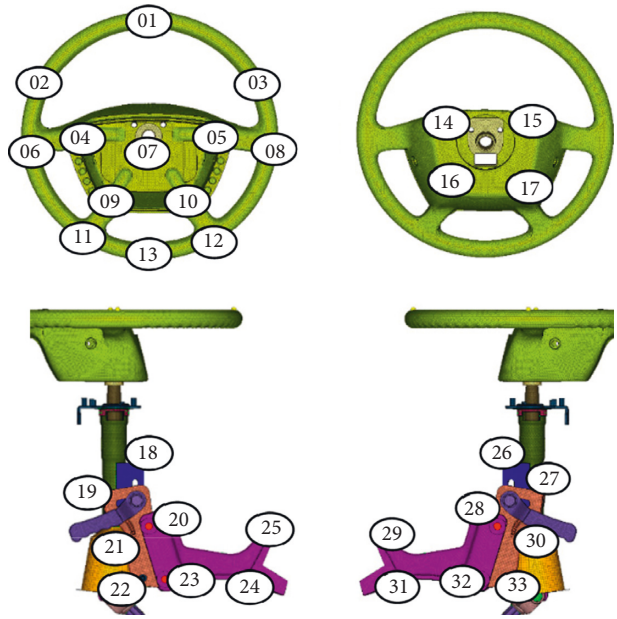

Figure 16: Distribution of the measuring points on the extracted steering model.

between adjacent nodes, the vibration system no longer considers the effect of external forces after being excited by the initial load, but the nodes are regarded an independent mass block connected by hinge points. Therefore, in the combined coupling characteristics of vibration, the steering system can be equivalent to an undamped multi-degree-of-freedom forced vibration system, the structure is equivalent to an equivalent mass block, and the mass blocks between each other are connected in series depending on the stiffness hinges (k_i), as shown in Figure 19.

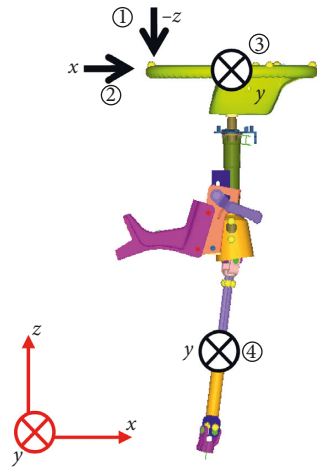

Figure 17: Position and direction of the hammer in the local coordinate system.

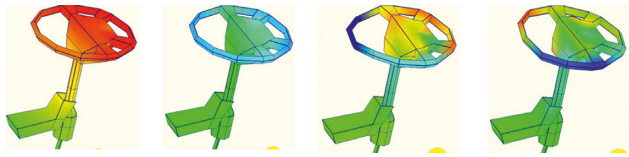

(24.2 Hz) (31.1 Hz) (40.6 Hz) (48.2 Hz)

Figure 18: Modal modes and frequencies of the steering system under hammer impact.

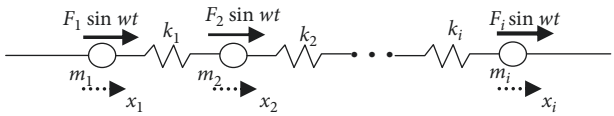

Figure 19: Equivalent undamped multi-degree-of-freedom vibration system for the steering system.

In Figure 19, $F_i \sin t$ (i is a positive integer) is the attenuated vibration forces transmitted under the periodic vibration excitation of the engine, m_i is the mass of the steering system member determined by the nodes on both sides of item i, and x_i is the displacement of each mass block in its respective relative coordinates. The corresponding undamped forced vibration equation can be obtained as follows:

$$\mathrm{M}\ddot{X} + \mathrm{K}X = F \sin wt,$$

$$M = \begin{bmatrix} m_1 & & & \\ & m_2 & & \\ & & \cdots & \\ & & & m_i \end{bmatrix},$$

$$K = \begin{bmatrix} k_1 & & & \\ & k_2 & & \\ & & \cdots & \\ & & & k_i \end{bmatrix}, \tag{19}$$

$$F = (F_1, F_2, \ldots, F_n)^T.$$

Because of the interaction force coupling among the mass blocks, the transposition matrix A_q of the mode shape matrix can be used to solve the decoupling problem as follows:

$$X = A_q X_q,$$
$$\ddot{X} = \mathrm{A}\ddot{X}_q. \tag{20}$$

After incorporating human characteristics, the decoupling expression is as follows:

$$A_q^T \mathrm{M} A_q \ddot{X}_p + A_q^T \mathrm{K} A_q X_p = A_q^T F \sin wt. \tag{21}$$

According to the regularization analysis, the displacement response of each regular coordinate under forced vibration of a single-degree-of-freedom system can be obtained:

$$x_{qi} = \frac{f_{Qi}}{w_S^2} \times \frac{1}{1 - (w_S/w_i)^2} \sin wt, \quad i = 1, 2, 3, \ldots, n, \tag{22}$$

$$w_i = \frac{1}{2\pi} \sqrt{\frac{k}{m}}, \tag{23}$$

where f_{Qi}, the amplitude of the exciting force, is subjected to i node; w_E is the ignition excitation frequency of the engine; and w_i is the natural frequency of the i item. Equation (21) shows that having the ignition excitation frequency of the engine close to the natural frequency of the rigid member can easily cause the resonance of the rigid part, causing greater jitter. Therefore, combining with equation (22) shows that reasonable arrangement of the mass and stiffness of the rigid member can easily make the natural frequency of the rigid member to deviate from the ignition excitation frequency of the the engine and avoid the occurrence of resonance. Therefore, a design scheme for vibration reduction of steering fixed support in abnormal vibration range is further proposed, just as shown in Figure 20.

Compared with the original steering support structure, the improvement scheme increases the thickness x of the steering support to x_1, and the distance between the stiffener plate and the mounting slot hole is also adjusted from z to z_1. These changes have been shown to significantly increase the radial stiffness value of the steering fixed support [41]. In addition, the mass of the original structure is also reduced, which is consistent with the lightweight design requirements of the steering fixed support. In addition, reducing the depth of the grooves and the use of discrete stiffened plate structures help reduce the stress concentration distribution, as shown in Figure 21.

In Figures 21(a) and 21(b), δ is the stiffness of the original stiffened plate, δ_0 and δ_1 are the discrete stiffnesses of the small dispersed stiffened plate, f_i', $i = 1, 2, \ldots, 5, 6$, is the stress concentration area at the warpage, and f_i, $i = 1, 2, \ldots, 5, 6$, is the improved stress dispersion area. Based on the original steering bearing structure, the improved design of the steering bearing further discretises its stiffness and analyzes the durability of the structure under the premise of reducing its own thickness. The improved model reference design indicators for the design can be summarised as follows:

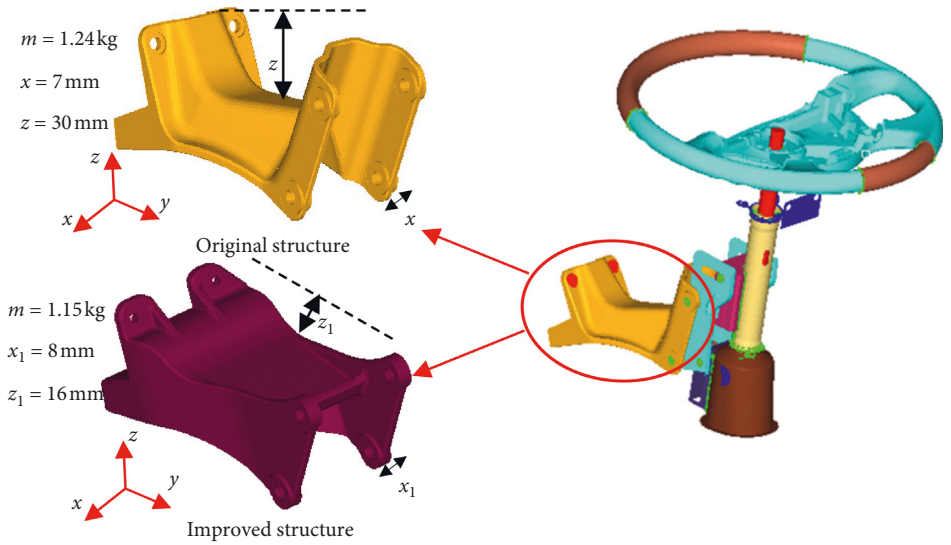

FIGURE 20: Comparison of the improved designs of the steering fixed support.

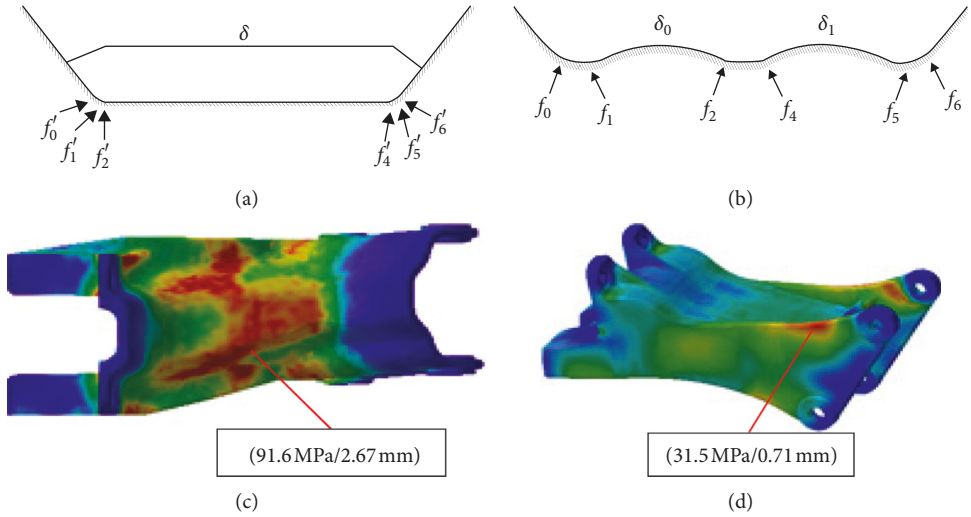

FIGURE 21: The comparison of original and improved structures. (a) The stress distribution of the original steering support structure, (b) the stress distribution of the improved structure, (c) the torsional stress analysis of the original structure, and (d) the torsional stress analysis of the improved structure.

$$\begin{aligned}
&\delta = \delta_0 + \delta_1 + \ldots + \delta_i, \quad i \le i_0(x, y, z),\\
&\frac{\partial(f_0', f_1', \ldots, f_5', f_6')}{\partial_x} + \frac{\partial(f_0', f_1', \ldots, f_5', f_6')}{\partial_y}\\
&+ \frac{\partial(f_0', f_1', \ldots, f_5', f_6')}{\partial_z} = 0,\\
&\frac{\partial(f_0, f_1, \ldots, f_5, f_6)}{\partial_x} + \frac{\partial(f_0, f_1, \ldots, f_5, f_6)}{\partial_y}\\
&+ \frac{\partial(f_0, f_1, \ldots, f_5, f_6)}{\partial_z} = 0,\\
&x_{\min} \le x \le x_{\max},\\
&y_{\min} \le y \le y_{\max},\\
&z_{\min} \le z \le z_{\max},
\end{aligned} \tag{24}$$

where $i_0(x, y, z)$ is the maximum number of discrete stiffness plates defined by the distributed dimension values (x, y, z) of the steering fixed bearing structure in three directions. According to the stress analysis of the structure of the steering fixed support before and after the improvement in Figures 21(c) and 21(d), the radial pressure of stress and strain values decreased, verifying the theoretical analysis above. To verify the inherent characteristics of the improved steering model, the modal simulation analysis was performed using the established simulation model.

4.4. Comparative Verification of Model before and after Optimization. Based on the established finite element model, with reference to the constraint mode of the solid part, the circumferential constraint of the model, and the degree-of-freedom constraint of the hinge point, the improved simulation model of the structure was compared and

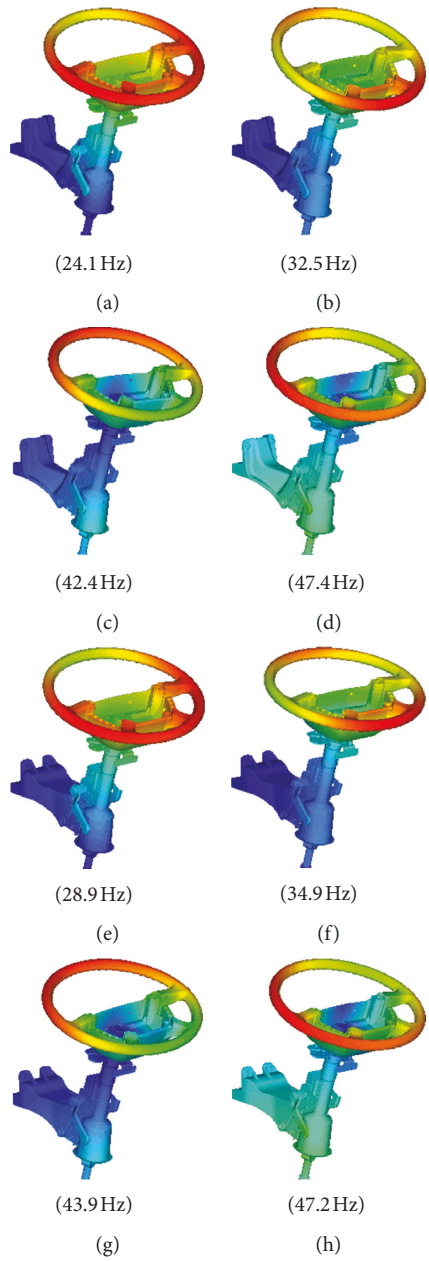

Figure 22: Comparison and analysis of the traditional model and improved model: (a)–(d) the first–fourth-order finite element modal of the traditional model and (e)–(h) is the first–fourth-order finite element modal of the improved model, respectively.

verified by modal analysis. The results are shown in Figure 22.

The analysis results of Figure 22 show that the modal of the previous order of the traditional steering model is consistent with the modal results of the test after applying the hammering method, showing the accuracy of the model. In addition, because the first-order modal frequency of the original structure is close to the ignition excitation frequency (23.3–25 Hz) of the engine, the whole steering structure is easy to produce resonance, leading to the aggravation of the vibration. Correspondingly, the modal frequency of the improved steering model and the excitation frequency of the engine produce a large degree of deviation (far away from the engine excitation frequency of $\sqrt{2}$ times), which accords with the initial frequency design requirements. Thus, the possibility of resonance is greatly avoided.

5. Experimental Verification

To verify the effectiveness of the improvement measures, the corresponding tests of the steering wheel before and after the improvement are, respectively, applied to evaluate and analyze the changing trend of the steering wheel vibration before and after the improvement. Because the vibration response at the edge of the steering wheel is more sensitive, take the measuring point on the upper end of the steering wheel as an example, and extract the equivalent vibration response spectrum curve of the steering wheel at

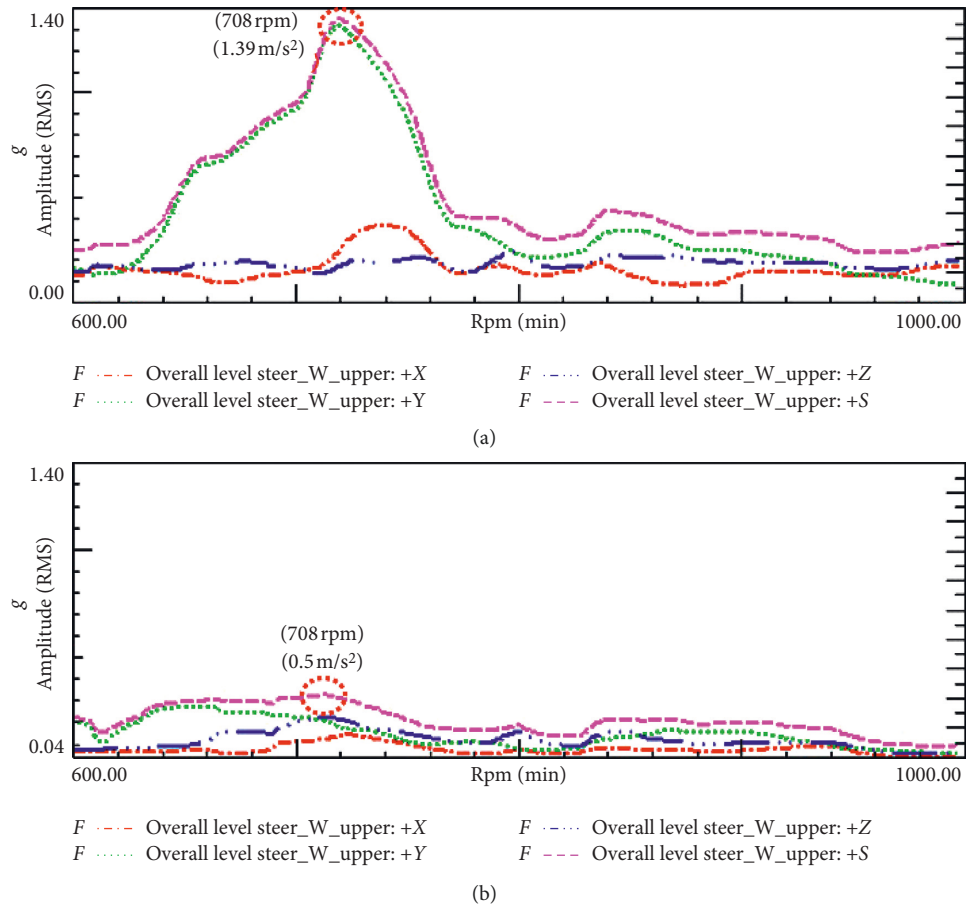

Figure 23: The vibrational spectrum of the upper end of the steering wheel in three directions: (a) vibration response of original steering wheel; (b) the vibration response of steering wheel after the improvement (sampled by per minutes).

the corresponding excitation frequency, as shown in Figure 23.

In Figure 23, +S ($a_s = (a_x^2 + a_y^2 + a_z^2)^{0.5}$) represents the total weighted acceleration value of the accelerometer in the X, Y, and Z directions. From the variation trend of the vibration RMS value of Figures 23(a) and 23(b) with the rotational speed, it can be seen that, under the resonance speed (700 rpm or so), the vibration RMS value of the upper end of the steering wheel after optimization is significantly lower than that before optimization, and the vibration RMS value of the upper end of the steering wheel before optimization has decreased sharply by 64% (from 1.39 m/s^2 to 0.5 m/s^2). In addition, from the RMS trend of the improved structure, it can be seen that the peak value of RMS meets the designed standard value (1.0 m/s^2), which indicates that the natural frequency of the improved structure has been shifted and effectively avoided the idle resonance frequency band, thus eliminating the problem of vibration aggravation caused by resonance and validating the effectiveness of the analysis method and improvement measures.

6. Conclusions

This paper proposes an MDVC method for the idle jitter problem of the steering wheel, mainly aims at the analysis of the vibration transmission path of the response object, and summarizes the characteristic attributes of the node transfer in the vibration transmission process of each ergodic subsystem, along with extracting the characteristics of the subsystem system on the vibration path and improving it with its adaptability. In the idling environment, the vibration of the structure mainly comes from the transmission of vibration and its own resonance effect. However, these are also related to the distribution forms of the structure, vibration disturbance of discrete parts in structure, and influence of node contact impact transfer between different subsystems. Aiming at the vibration path characteristics of the steering wheel, the real vehicle test focused on these divided systems of nodes was performed, and the test shows that the self-excited resonance effect of the steering node system is the possible cause of the abnormal vibration of the steering wheel, along with the corresponding abnormal idle speed intervals concentrated between 700 rpm and 750 rpm. To avoid the disturbance of factors from other subsystems, the steering system model was extracted from the real vehicle, and the vibration mode of the original steering system was tested by the hammer method, and the specific reasons for the abnormal vibration were determined. Furthermore, an improved steering support structure was proposed, and

the fit degree between the simulation model and the solid model was verified by the finite element combination analysis method. At the same time, the difference of the steering modes before and after optimization was compared. Thus, the mode of the steering system deviates from the excitation frequency of the engine and avoids the resonance problem. Lastly, the test results show that the vibration of the steering wheel decreased, verifying the effectiveness of the improved method. However, for the vibration control, in addition to the vibration reduction design scheme of the polarization frequency and vibration avoidance, the arrangement of the discrete structure in the node system and the influence of the tilt angle of the components between the node systems, along with the additional node displacement deviation caused by the modal resonance between the system components on the vibration isolation effect, need to be further studied and analyzed in the future.

Notations

N_{i+6}: Measuring point (nodes) on the responds object
N_{i+5}: Coupling nodes to upper associated systems in node system 4
N_{i+4}: Indirect connection points to upper associated systems in node system 3
N_{i+3}: Coupling nodes to upper associated systems in node system 3
N_{j+4}: Coupling nodes to upper associated systems and symmetrical with N_{i+4}
N_{j+3}: Indirect connection points to upper associated systems and symmetrical with N_{i+3}
N_{i+1}, N_{i+2}, N_{j+2}, N_{j+1}: Coupling nodes to upper associated systems in node system 2
N_0: Measuring point (nodes) on the excitation source
w_{ni}: The natural frequency of the i-th mode
Δx_v, Δx_1, Δx_2, Δx_3, Δx_R: Displacement offset of the node system
R: The root-mean-square values of vibration weighted acceleration of the transfer node
N_1, N_2, N_3: Coupling nodes to upper associated systems in node system 4
N_4: Indirect connection points to upper associated systems in node system 3
N_i, N_j: Coupling nodes in associated systems
V_A: Vibration velocity response of the structural ontology
H_A: The admittance transfer function
F_A: The exciting force
n_1, n_2, n_3: The engine mounting nodes
a_p: The vibration RMS value of the engine body
a_{n1}: The vibration RMS values of the front mount of the engine
φ_i: The phase angle of the i-th mode
m_1, m_2, m_3, m_R: The mass of the each node system
w_s: The excitation frequency of an engine at a certain speed
a_i: The root-mean-square (RMS) value of acceleration
a_w: The vibration acceleration time-domain signal
T: The recorded acceleration time
X_i: The kinematic displacement solution
A_i: Displacement response amplitude
f_{si}: The frequency of the ignition pulse vibration excitation
a_{n2}: RMS values of the left rear mount of the engine
δ_t: The vibration isolation rate
τ: The number of strokes of the engine
n: Idle speed
a_{n3}: The vibration RMS value of the right rear mount of the engine
δ_1, δ_2, δ_3, δ_R: Additional vibration displacement under the mutual coupling of the excitation frequency of the engine
k_1, k_2, k_3, k_R: The stiffness of the node system
w_i: The proximity value of the natural frequency of a node system
c_i: Effective constrained damping value
k_i: Effective constrained stiffness value
m_i: Mass value of node system i
x_i: The displacement of each mass block in its respective relative coordinates
A_q: Mode shape matrix
X_q: Modal coordinate transformation matrix
X: Modal deformation
f_{Qi}: The amplitude of the exciting force
x: The thickness of the steering support
z: The distance between the stiffener plate and the mounting slot hole
δ: The stiffness of the original stiffened plate
δ_0, δ_1: The discrete stiffnesses of the small dispersed stiffened plate
f_i', $i = 1, 2, \ldots, 5, 6$: The stress concentration area at the warpage
f_i, $i = 1, 2, \ldots, 5, 6$: The improved stress dispersion area
$i_0(x, y, z)$: The maximum number of discrete stiffness plates.

Data Availability

The data used to support the findings of this study are available from the corresponding author upon request.

Conflicts of Interest

The authors declare that there are no conflicts of interest regarding the publication of this paper.

Acknowledgments

This research was financially supported by the Project of National Natural Science Foundation of China (Grant no. 51965013), Science and Technology Major Project of Guangxi (Grant nos. AA18242033 and AA18242036), Guangxi Key Laboratory of Manufacture System and Advanced Manufacture Technology (Nos. 17-259-05-009Z and 17-259-05-010Z), GUET Excellent Graduate Thesis (Grant no. 17YJPYSS02), and Innovation Project of GUET Graduate Education (Grant no. 2019YCXS001).

References

[1] X. Sun, H. Zhang, W. Meng, R. Zhang, K. Li, and T. Peng, "Primary resonance analysis and vibration suppression for the harmonically excited nonlinear suspension system using a pair of symmetric viscoelastic buffers," *Nonlinear Dynamics*, vol. 94, no. 2, pp. 1243–1265, 2018.

[2] J. Lim, W. Sim, S. Yun, D. Lee, and J. Chung, "Reduction of vibration forces transmitted from a radiator cooling fan to a vehicle body," *Journal of Sound and Vibration*, vol. 419, pp. 183–199, 2018.

[3] R. Wang, J. Huang, and B. Wei, "Test investigation on the vibration of steering wheel under idling based on LMS," *Journal of Zhengzhou University (Engineering Science)*, vol. 3, p. 19, 2016.

[4] J. S. Chen and H. Y. Hwang, "Steering test of mid-size bus with flexible-body dynamics model," *MATEC Web of Conferences*, vol. 169, p. 01038, 2018.

[5] S. Dutta and S.-B. Choi, "Control of a shimmy vibration in vehicle steering system using a magneto-rheological damper," *Journal of Vibration and Control*, vol. 24, no. 4, pp. 797–807, 2018.

[6] D. Lee, K.-S. Kim, and S. Kim, "Controller design of an electric power steering system," *IEEE Transactions on Control Systems Technology*, vol. 26, no. 2, pp. 748–755, 2018.

[7] G. Wittler, M. Haßenberg, H. Henrichfreise, H. Briese, and T. Schubert, *Systematic Model-Based Vibration Analysis of a Controlled Electric Power Steering System*, Springer Vieweg Verlag, in *Proceedings of the 8th International Munich Chassis Symposium 2017*, pp. 505–517, Springer Vieweg Verlag, Wiesbaden, Germany, 2017.

[8] P. A. Savta and P. H. Jain, "A study of reduction in the vibrations of steering wheel of agricultural tractor," *Journal of Engineering Research and Application*, vol. 6, pp. 80–87, 2016.

[9] L. H. Zheng, Z. Liu, M. L. Chen, and Y. T. Zhu, "Vibration modeling and position-dependent analysis of spatial trajectory roller coaster," *Archive of Applied Mechanics*, vol. 87, no. 3, pp. 489–502, 2017.

[10] T. L. M. Djomo Mbong, M. Siewe Siewe, and C. Tchawoua, "The effect of nonlinear damping on vibrational resonance and chaotic behavior of a beam fixed at its two ends and prestressed," *Communications in Nonlinear Science and Numerical Simulation*, vol. 22, pp. 1–3, 2015.

[11] S. Saghir and M. I. Younis, "An investigation of the static and dynamic behavior of electrically actuated rectangular microplates," *International Journal of Non-linear Mechanics*, vol. 85, pp. 81–93, 2016.

[12] D. M. El-Gazzar, "Finite element analysis for structural modification and control resonance of a vertical pump," *Alexandria Engineering Journal*, vol. 56, no. 4, pp. 695–707, 2017.

[13] A. Tullu, Y. Byun, J.-N. Kim, and B.-S. Kang, "Parameter optimization to avoid propeller-induced structural resonance of quadrotor type unmanned aerial vehicle," *Composite Structures*, vol. 193, pp. 63–72, 2018.

[14] M. Tompkins, R. Stakenborghs, and G. Kramer, "Use of FEA software in evaluating pump vibration and potential remedial actions to abate resonance in industrial vertical pump/motor combinations," in *Proceedings of the 2016 24th International Conference on Nuclear Engineering (ICONE24)*, pp. 26–30, Charlotte, NC, USA, 2016.

[15] A. S. Genikomsou and M. A. Polak, "Finite element analysis of punching shear of concrete slabs using damaged plasticity model in ABAQUS," *Engineering Structures*, vol. 98, pp. 38–48, 2015.

[16] Y. Huang, L. J. Yang, X. Z. Du, and Y. P. Yang, "Finite element analysis of thermal behavior of metal powder during selective laser melting," *International Journal of Thermal Sciences*, vol. 104, pp. 146–157, 2016.

[17] Y. Morimoto, A. Takagi, M. Ueki, and L. Pirsig, "Vibration modal analysis by high-speed and accurate shape measurement using one-pitch phase analysis method," *Advancement of Optical Methods & Digital Image Correlation in Experimental Mechanics*, vol. 3, pp. 103–108, 2019.

[18] H. Yin, F. Ma, X. Zhang, C. Gu, H. Gao, and Y. Wang, "Research on equivalent material properties and modal analysis method of stator system of permanent magnet motor with concentrated winding," *IEEE Access*, vol. 7, pp. 64592–64602, 2019.

[19] I. J. Myung, "The importance of complexity in model selection," *Journal of Mathematical Psychology*, vol. 44, no. 1, pp. 190–204, 2000.

[20] N. Shehzad, A. Zeeshan, R. Ellahi, and K. Vafai, "Convective heat transfer of nanofluid in a wavy channel: buongiorno's mathematical model," *Journal of Molecular Liquids*, vol. 222, pp. 446–455, 2016.

[21] X. Zhan, J. Xu, and H. Fang, "Planar locomotion of a vibration-driven system with two internal masses," *Applied Mathematical Modelling*, vol. 40, no. 2, pp. 871–885, 2016.

[22] B.-L. Zhang, Q.-L. Han, and X.-M. Zhang, "Recent advances in vibration control of offshore platforms," *Nonlinear Dynamics*, vol. 89, no. 2, pp. 755–771, 2017.

[23] W. He, X. He, M. Zou, and H. Li, "PDE model-based boundary control design for a flexible robotic manipulator with input backlash," *IEEE Transactions on Control Systems Technology*, vol. 99, pp. 1–8, 2018.

[24] S. Mondal, A. Yadav, R. Kumar et al., "Molecular-level structural insight into clarified oil by nuclear magnetic resonance (NMR) spectroscopy: estimation of hydrocarbon types and average structural parameters," *Energy & Fuels*, vol. 31, no. 7, pp. 7682–7692, 2017.

[25] Y. B. Yang and J. D. Yau, "Vertical and pitching resonance of train cars moving over a series of simple beams," *Journal of Sound and Vibration*, vol. 337, pp. 135–149, 2015.

[26] W. Yu-Jen, C. Tsung-Yi, and Y. Jui-Hsin, "Design and kinetic analysis of piezoelectric energy harvesters with self-adjusting resonant frequency," *Smart Materials and Structures*, vol. 26, no. 9, Article ID 095037, 2017.

[27] W. Sun, J. Zhou, D. Gong, and T. You, "Analysis of modal frequency optimization of railway vehicle car body," *Advances in Mechanical Engineering*, vol. 8, no. 4, 2016.

[28] B. He, W. Tang, S. Huang, S. Hou, and H. Cai, "Towards low-carbon product architecture using structural optimization for lightweight," *The International Journal of Advanced*

Manufacturing Technology, vol. 83, no. 5–8, pp. 1419–1429, 2016.

[29] W. Torres, J. L. Almazán, C. Sandoval, and R. Boroschek, "Operational modal analysis and FE model updating of the Metropolitan Cathedral of Santiago, Chile," *Engineering Structures*, vol. 143, pp. 169–188, 2017.

[30] M. Nouri, B. Nasehi, S. Abdanan, M. Mehdizadeh, and M. A. Goudarzi, "A novel application of vibration technique for non-destructive evaluation of bread staling," *Journal of Food Engineering*, vol. 197, pp. 44–47, 2017.

[31] Z.-W. Wang and L.-J. Wang, "On accelerated random vibration testing of product based on component acceleration RMS-life curve," *Journal of Vibration and Control*, vol. 24, no. 15, pp. 3384–3399, 2018.

[32] S. Cankaya, A. Koyuncu, and M. Balaban, "Steering wheel idle vibration improvement on tractor, Sigma," *Journal of Engineering & Natural Sciences/Mühendislik Ve Fen Bilimleri Dergisi*, vol. 34, no. 1, 2016.

[33] J. Igba, K. Alemzadeh, C. Durugbo, and E. T. Eiriksson, "Analysing RMS and peak values of vibration signals for condition monitoring of wind turbine gearboxes," *Renewable Energy*, vol. 91, no. 3, pp. 90–106, 2016.

[34] Z. Lu, M. J. Brennan, and L.-Q. Chen, "On the transmissibilities of nonlinear vibration isolation system," *Journal of Sound and Vibration*, vol. 375, pp. 28–37, 2016.

[35] I. L. Ladipo, J. D. Fadly, and W. F. Faris, "Characterization of magnetorheological elastomer (MRE) engine mounts," *Materials Today: Proceedings*, vol. 3, no. 2, pp. 411–418, 2016.

[36] J. T. Song, S. J. Ahn, W. B. Jeong, and W. S. Yoo, "Subjective absolute discomfort threshold due to idle vibration in passenger vehicles according to sitting posture," *International Journal of Automotive Technology*, vol. 18, no. 2, pp. 293–300, 2017.

[37] M. Amabili, F. Alijani, and J. Delannoy, "Damping for large-amplitude vibrations of plates and curved panels, part 2: identification and comparisons," *International Journal of Non-linear Mechanics*, vol. 85, pp. 226–240, 2016.

[38] F. Alijani, M. Amabili, P. Balasubramanian, S. Carra, G. Ferrari, and R. Garziera, "Damping for large-amplitude vibrations of plates and curved panels, part 1: modeling and experiments," *International Journal of Non-linear Mechanics*, vol. 85, pp. 23–40, 2016.

[39] Z. Wang, Y. Jiao, and Z. Chen, "Parameter study of friction damping ring for railway wheels based on modal analysis," *Applied Acoustics*, vol. 153, pp. 140–146, 2019.

[40] H. Cui, X. Xu, W. Peng, Z. Zhou, and M. Hong, "A damage detection method based on strain modes for structures under ambient excitation," *Measurement*, vol. 125, pp. 438–446, 2018.

[41] X. Yin, W. Wu, K. Zhong, and H. Li, "Dynamic stiffness formulation for the vibrations of stiffened plate structures with consideration of in-plane deformation," *Journal of Vibration and Control*, vol. 24, no. 20, pp. 4825–4838, 2018.